Topology Optimization of Antennas and Waveguide Transitions

Emadeldeen Hassan

PhD thesis, 2015
Department of Computing Science
Umeå University
SE-901 87 Umeå
Sweden

Department of Computing Science
Umeå University
SE-901 87 Umeå
Sweden

UMINF: 15.07
ISSN: 0348-0542
ISBN: 978-91-7601-255-0

Cover picture: Courtesy of NASA/JPL-Caltech

Electronic version available at http://umu.diva-portal.org/
Printed by Print & Media, Umeå University
Umeå, Sweden 2015

Abstract

This thesis introduces a topology optimization approach to design, from scratch, efficient microwave devices, such as antennas and waveguide transitions. The design of these devices is formulated as a general optimization problem that aims to build the whole layout of the device in order to extremize a chosen objective function. The objective function quantifies some required performance and is evaluated using numerical solutions to the 3D Maxwell's equations by the finite-difference time-domain (FDTD) method. The design variables are the local conductivity at each Yee edge in a given design domain, and a gradient-based optimization method is used to solve the optimization problem. In all design problems, objective function gradients are computed based on solutions to adjoint-field problems, which are also FDTD discretization of Maxwell's equations but solved with different source excitations. For any number of design variables, the computation of the objective function gradient requires one solution to the original field problem and one solution to the associated adjoint-field problem. The optimization problem is solved iteratively using the globally convergent Method of Moving Asymptotes (GCMMA).

By the proposed approach, various design problems, including tens of thousands of design variables, are formulated and solved in a few hundred iterations. Examples of solved design problems are the design of wideband antennas, dual-band microstrip antennas, wideband directive antennas, and wideband coaxial-to-waveguide transitions. The fact that the proposed approach allows a fine-grained control over the whole layout of such devices results in novel devices with favourable performance. The optimization results are successfully verified with a commercial software package. Moreover, some devices are fabricated and their performance is successfully validated by experiments.

Sammanfattning

Denna avhandling introducerar en topologioptimeringsmetod för att, från grunden, utforma effektiva mikrovågsenheter, som exempelvis antenner och vågledarövergångar. Problemet att utforma dessa enheter formuleras här som ett optimeringsproblem som syftar till att bestämma hela layouten för enheten med avsikt att minimera eller maximera en vald målfunktion. Denna målfunktion kvantifierar önskade prestanda och utvärderas med hjälp av numeriska finita-differens tidsdomänslösningar (FDTD) till Maxwells ekvationer i 3D. Designvariablerna är den lokala konduktiviteten för varje kant i beräkningsnätet i ett givet designområde och en gradientbaserad optimeringsmetod löser optimeringsproblemet. I alla utformningsproblem beräknas målfunktionens gradient med hjälp av lösningar till ett adjungerat fältproblem, som också är en FDTD-diskretisering av Maxwells ekvationer men med en annan excitation. Oavsett antalet designvariabler, kräver beräkningen av målfunktionsgradienten en lösning till det ursprungliga fältproblemet samt en lösning av det adjungerade fältproblemet. Optimeringsproblemet löses iterativt med den globalt konvergenta versionen av optimeringsmetoden MMA (Method of Moving Asymptotes).

Med användning av den föreslagna metoden formuleras och löses ett flertal olika designproblem med tiotusentals designvaribler i ett par hundra iterationer. Till exempel utformas plana bredbandsantenner, dubbelbands mikrostripantenner, riktade bredbandsantenner, samt bredbandiga övergångar från koaxialkablar till vågledare. Det faktum att den föreslagna metoden tillåter en detaljerad kontrol över utformningen av enheterna möjliggör nyskapande utformningar med utmärkta prestanda. Förutom att korsvalidera prestandan av de optimerade enheterna med ett kommersiellt mjukvarupaket så har några av de optimerade enheterna även tillverkats, och deras prestanda har utvärderats experimentellt med resultat som väl överensstämmer med de beräknade.

Acknowledgements

First and foremost, I am thankful to Allah, the most gracious most merciful.

I am grateful to my scientific advisor Martin Berggren for his great guidance, support, and invaluable knowledgeable discussions. I would like to extend my deepest thanks to Eddie Wadbro for the fruitful discussions not only on research but on many areas in life, as well. I also like to express my deep thanks to Daniel Noreland for the valuable discussions. I thank an anonymous person who is keen to share his knowledge.

I would like to thank my colleagues in the design and optimization group, my colleagues at UMIT research lab, and my colleagues at the department of computing science, for the friendly working environment.

I find no words that can express my gratitude to my parents, and I ask Allah to reward them.

I appreciate my wife, who was keen to create and give all kind of support during this work.

The PhD work was in part supported financially by the Swedish Research Council. The computations were performed on resources provided by the Swedish National Infrastructure for Computing (SNIC) at the center for scientific and technical computing at Lund University (Lunarc) and at the High Performance Computing Center North (HPC2N) at Umeå University.

Preface

This thesis consists of an introductory chapter and the following papers:

I. Emadeldeen Hassan, Eddie Wadbro, and Martin Berggren, *Topology optimization of UWB monopole antennas*, In 7^{th} European Conference on Antennas and Propagation (EuCAP2013), 1429–1433, Gothenburg, Sweden, Apr. 2013.

II. Emadeldeen Hassan, Eddie Wadbro, and Martin Berggren, *Topology optimization of metallic antennas*, IEEE Transactions on Antennas and Propagation, vol. 62, no. 5, pp. 2488-250, May 2014.

III. Emadeldeen Hassan, Eddie Wadbro, and Martin Berggren, *Patch and ground plane design of microstrip antennas by material distribution topology optimization*, Progress in Electromagnetics Research B, vol. 59, pp. 89-102, 2014.

IV. Emadeldeen Hassan, Daniel Noreland, Robin Augustine, Eddie Wadbro, and Martin Berggren, *Topology Optimization of Planar Antennas for Wideband Near-Field Coupling*, submitted.

V. Emadeldeen Hassan, Eddie Wadbro, and Martin Berggren, *Time-Domain Sensitivity Analysis for Conductivity Distribution in Maxwell's Equations*, Dept. of Computing Science, Umeå University, Technical Report UMINF 15.06, 2015.

VI. Emadeldeen Hassan, Daniel Noreland, Eddie Wadbro, and Martin Berggren, *Topology Optimization of Coaxial-to-Waveguide Transitions*, submitted.

1 Introduction

1.1 Motivation

The complexity of emerging wireless systems raises the demands on antenna designs. Examples of such demands are multi-frequency band operation, compactness, and reduced energy consumption. Moreover, there is a growing interest in using microwaves in detection and imaging systems. Microwave imaging can either complement or replace some of the currently used imaging systems. The design of proper antennas is a key element for such systems to function efficiently.

1.2 Antenna concepts

Antennas are the parts of transmitting or receiving systems that can radiate or receive electromagnetic waves [1]. Usually, antenna characteristics are described in the frequency domain. The concept of antenna radiation can be illustrated with the simplified model shown in Figure 1. A signal source V_s launches voltage and current waves (V^{inc}, I^{inc}) that propagate along a lossless transmission line. The transmission line has a real characteristic impedance Z_{c} that may depend on the frequency f. Examples of transmission lines are coaxial cables, waveguides, striplines, and microstrip lines [2]. An ideal antenna should accept all the incident waves (V^{inc}, I^{inc}), that is, the reflected waves (V^{ref}, I^{ref}) back to the source should be zero, and convert all the accepted waves to electromagnetic waves ($\boldsymbol{E}$, $\boldsymbol{H}$) in a surrounding medium with intrinsic impedance η.

An antenna connected to the end of a transmission line is seen by the transmission line as a load with a frequency dependent impedance Z_{a}. For an antenna to radiate ideally, the antenna equivalent impedance, Z_{a}, should satisfy two conditions. Firstly, the impedance Z_{a} should introduce no ohmic losses. Secondly, the impedance Z_{a} should equal the transmission line impedance Z_{c} in the operational frequency band in order to maximize the radiated power. The first condition might be satisfied by using materials with very low ohmic losses, such as good conductors or good dielectrics. The second condition is typically fulfilled by finding a suitable structure, which generally has physical dimensions related to the frequency of operation. Finding suitable antenna structures is the goal for most antenna design problems.

Standard antennas have structures that can take on a variety of physical forms. They can be as simple as a single radiating dipole, or far more complicated structures consisting of two-dimensional or three-dimensional geometric shapes [3]. Figure 2 shows some standard antenna configurations. Generally, the characteristics of the radiated electromagnetic waves depend on the antenna configuration.

Antenna characteristics can be roughly divided into near-field characteristics and far-field characteristics. Two of the commonly used near-field characteristics are the *reflection coefficient* and the *radiation efficiency*. The antenna reflection coefficient, S_{11}, can be defined as the ratio of the amplitudes of the reflected and incident voltage waves at the antenna terminal,

$$S_{11} = \frac{V_{\text{a}}^{\text{ref}}}{V_{\text{a}}^{\text{inc}}}. \tag{1}$$

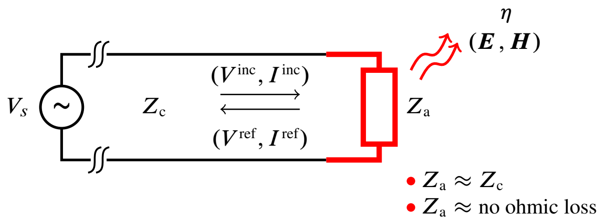

Figure 1: A simplified model of an antenna, Z_{a}, connected to a lossless transmission line with characteristic impedance Z_{c}.

A reference value of $|S_{11}| = -10$ dB, that is, $20\log_{10}|S_{11}| = -10$, is conventionally used by antenna engineers as an upper bound to express satisfactory antenna performance. The antenna *input impedance* Z_{a} is related to the reflection coefficient at the antenna terminal through the expression

$$Z_{\mathrm{a}} = Z_{\mathrm{c}}\frac{1+S_{11}}{1-S_{11}}. \tag{2}$$

Note that when S_{11} is zero, the antenna and the transmission line are matched, that is, $Z_{\mathrm{a}} = Z_{\mathrm{c}}$. However, the use of the reflection coefficient (or the input impedance) alone to evaluate the antenna radiation can be misleading, since lossy antennas can be easily matched to the transmission line. The antenna radiation efficiency, e, accounts for the amount of power loss inside the antenna structure. The radiation efficiency, e, is defined as

$$e = \frac{P^{\mathrm{rad}}}{P^{\mathrm{rad}} + P^{\mathrm{loss}}}, \tag{3}$$

where P^{rad} and P^{loss} are the power radiated by the antenna and the power loss inside the antenna structure, respectively.

Two of the widely used far-field characteristics of an antenna are the *directivity* and the *field polarization*. The directivity measures the relative spatial distribution of the radiated power around the antenna. Directive antenna radiates more power in some directions than in others, which may be a requirement for some systems. The antenna polarization is an indication of the orientation of the radiated field (conventionally the electric field) in a certain direction.

1.3 Antenna analysis

The goal of antenna analysis is to determine some of the radiation characteristics for a given antenna structure. Generally, the interaction between electromagnetic waves and any structure can be predicted by the 3D Maxwell's equations together with constitutive laws for the materials involved. Hence, for antenna analysis, solutions to Maxwell's equations are needed. For linear, isotropic, and non-dispersive media, the differential form of Maxwell's equations

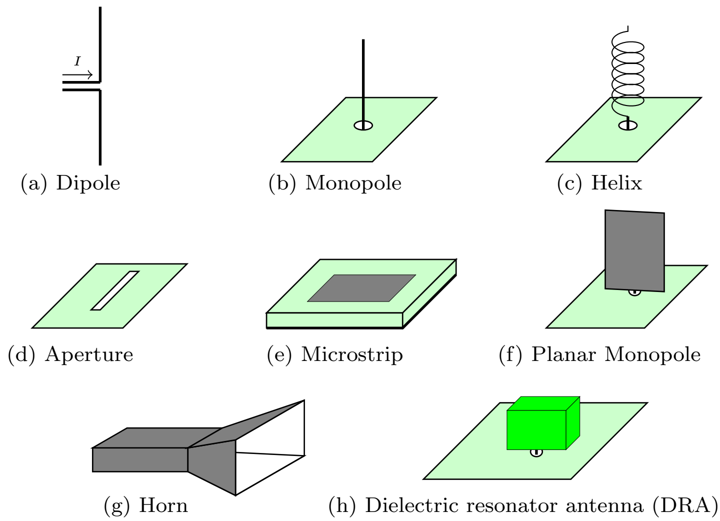

(a) Dipole (b) Monopole (c) Helix

(d) Aperture (e) Microstrip (f) Planar Monopole

(g) Horn (h) Dielectric resonator antenna (DRA)

Figure 2: Some standard antenna configurations.

can be written as

$$\frac{\partial}{\partial t}\mu \boldsymbol{H} + \nabla \times \boldsymbol{E} = \boldsymbol{0}, \tag{4a}$$

$$\frac{\partial}{\partial t}\epsilon \boldsymbol{E} + \sigma \boldsymbol{E} + \boldsymbol{J} - \nabla \times \boldsymbol{H} = \boldsymbol{0}, \tag{4b}$$

where $\boldsymbol{E}$, $\boldsymbol{H}$, and $\boldsymbol{J}$ are the electric field, the magnetic field, and the electric current source, respectively. The constitutive parameters μ, ϵ, and σ denote, respectively, permeability, permittivity, and conductivity of the medium. The antenna structure can be described directly through the constitutive parameters or implicitly by imposing suitable boundary conditions.

For simple antenna structures, such as dipoles or standard microstrip antennas, approximate solutions to Maxwell's equations can be used to obtain fast models that describe some antenna characteristics. However, for complex antenna structures, full-wave solutions to Maxwell's equations are required to obtain reliable analysis.

Currently, there are many accurate numerical methods that solve the 3D Maxwell's equation, such as the finite element methods (FEM), the method of moments (MoM), and the finite difference time domain (FDTD) method [4]. Each numerical method has advantages and limitations concerning the computational cost, the level of accuracy, and the material modelling. But generally, antenna radiation characteristics can be accurately predicted by using any of these methods.

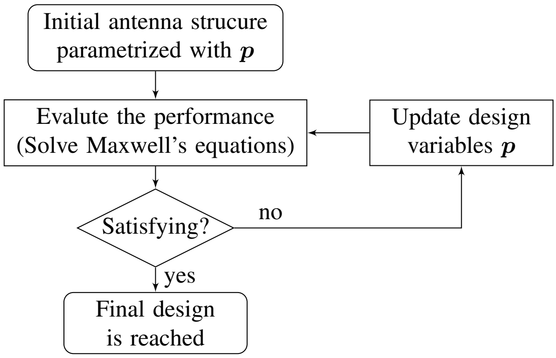

Figure 3: A general scheme for antenna design.

1.4 Antenna design

The aim of antenna design is to find a suitable antenna structure that satisfies certain design objectives. Usually, the design objectives are to improve some of the antenna radiation characteristics. For example, the antenna might be designed to radiate in different frequency bands, to achieve a certain far-field polarization, or to have a specific directivity. Figure 3 illustrates the basic scheme used for antenna design. A designer suggests an initial structure. The structure is then parameterized by a set of variables $\boldsymbol{p}$. The aim is to optimize these variables to achieve a satisfying performance. The optimization of the antenna is generally an iterative process. The performance of the suggested structure is evaluated, and if the performance is not satisfactory, the design variables are updated. The evaluation and update loop is repeated until either a satisfying performance is obtained or a certain number of iterations is reached. Generally, the result of the optimization depends critically on the initial structure, the way the structure is parameterized, and the strategy of updating the design variables.

There is a growing interest in formulating antenna design problems as mathematical optimization problems, where numerical solutions to Maxwell's equations and numerical optimization algorithms are combined to automate the design process. Thus, the design process comprises two major parts. On the one hand, numerical methods are used to analyze the antenna structure and to evaluate the formulated objective function. Moreover, additional computations are sometimes performed to evaluate derivatives of the objective function with respect to the design variables. On the other hand, optimization algorithms are used to update the design variables to improve the objective function.

Typically, a large portion of the computational time is consumed in the evaluation step. For simple antenna structures, the computational time might be reduced by space mapping techniques [5, 6]. In such techniques, dominating features of the antenna structure are mapped into a computationally fast, but less accurate, model often called a surrogate model. The optimization is carried out mainly using the surrogate model, with the possibility of updating that model during the optimization to align with the original problem and capture more physics. However, some antenna structures are too complex to lend their features to a surrogate model. Evaluation of such antennas, therefore, requires accurate solutions to Maxwell's equations, which are usually computationally expensive. Thus, when optimizing complex antennas, it is essential to use efficient optimization algorithms.

1.5 Optimization algorithms

Staring from an initial guess for the design variables, optimization algorithms seek a solution of a formulated optimization problem by generating a sequence of updated design variables. In each step of this procedure, optimization algorithms use the available information about the optimization problem to update the design variables in order to improve the objective function. In electromagnetic design problems, two classes of optimization algorithms are typically used: metaheuristics and gradient-based algorithms.

Metaheuristics are high-level problem-independent heuristic optimization algorithms that derive heuristic optimization strategies from a metaphor [7]. A metaphor might be a biological system, individual and collective behavior, or a physical process. Typical examples of metaheuristics are genetic algorithms, particle swarm optimization, and simulated annealing [8–11]. Metaheuristics only use information about the value of the objective function, which make them simple to use as a black-box software. In these algorithms, the design variables are updated using heuristics that typically include some stochastic parts. The stochastic parts allow these algorithms to avoid being trapped into a local optimum while searching for a solution. Because of their simplicity of use, these methods are frequently used in the electromagnetic community for design problems that are generally characterized by a small number of design variables [12–14]. Further, most of the commercial software packages used for electromagnetic analysis are provided with one or more of those optimization algorithms. However, the small amount of information contained in a usually sparse sampling of objective function values, together with the stochastic parts employed to update the design variables, make metaheuristics inefficient for optimization problems with a large number of design variables [15].

On the other hand, gradient-based optimization algorithms can efficiently handle optimization problems that have a large number of design variables. In gradient-based optimization algorithms, the design variables are updated based on the necessary conditions of optimality of the mathematical optimization problems. Information about the objective function and its derivatives with respect to the design variables are used to find the new updates. If the Hessian of the objective function (the matrix of second derivatives) is available to a low computational cost, optimization algorithms based on second derivatives, such as Newton methods, are preferred because of their fast local convergence. However, computing the Hessian of the objective function is often expensive, which is why optimization problems are often solved by first-order methods such as steepest descent, quasi-Newton, and sequential convex approximations methods [16, 17]. First-order methods, besides requiring the objective function value, require the gradient vector (the derivatives of the objective function with respect to the design variables). The objective function gradient can be evaluated by methods such as finite difference approximations and adjoint-field methods [18–26]. The latter, if accessible, are vastly more accurate and efficient to use, especially when the number of variables is large. Basic versions of gradient-based optimization algorithms are usually only locally convergent; that is, the algorithm will converge to a local optimum if it is initialized sufficiently close to that optimum. By adding a globalization strategy to a locally convergent algorithm, the algorithm can be made to converge to a local optimum regardless of the initial starting point [16].

Gradient-based optimization algorithms have been used to solve electromagnetic problems such as inverse scattering problems [18–23, 27, 28], filter designs [29–31], and optimization of magnetic devices [32–35]. However for antenna optimization problems, metaheuristics have dominated the scene, and only a few works have used gradient-based optimization algorithms [36–40]. One reason for this lack of progress is the difficulty in formulating the design problem as an optimization problem for which the gradient information can be computed in an efficient way. Another reason is the tendency of gradient-based methods to converge to local optima, and it may well happen that the optimization algorithm is trapped in a poor local optimum. Nevertheless, once the optimization problem is formulated, a well-designed gradient-based optimization algorithm will typically find at least a local optimum, which cannot be guaranteed if metaheuristics are used instead.

1.6 Topology optimization

Design optimization methods can be classified, based on the generality of how the design domain is parameterized, into three groups: sizing, shape, and topology optimization. In sizing optimization, a structure is parameterized by a set of design variables that express, for instance, height, width, or thickness of parts of the structure. In shape optimization, the design variables are used to parameterize the shape of the boundary of a given structure [13, 41–43].

The term topology optimization is often used to label the most general type of design optimization methods, in which the shapes as well as the connectivity of individual parts of the device are subject to design. In topology optimization, design variables are typically used to describe a function that can spatially describe any structure in one, two, or three dimensional space. The most common way of carrying out topology optimization, which is used in this thesis, is through the *material distribution approach*. This approach was originally developed to design load-carrying elastic structures [44–47], but the method has been successfully extended also to other physical disciplines such as acoustics and optics [48–51]. In this approach, a density function is used to express the distribution of a material in a given domain. Typically, the density function is sampled into a density vector $\boldsymbol{p} = [p_1, p_2, \cdots, p_M]$. Each component p_i of the density vector is assigned to an element i in the design domain to indicate presence, $p_i = 1$, or absence, $p_i = 0$, of a material. During the optimization of a particular objective function, the components of the density vector are allowed to take any value between 0 and 1, but by the end of the process the vector $\boldsymbol{p}$ must hold binary values only, that is, $p_i = 0$ or 1 for all i. Instead of optimizing directly over a density function, an alternative topology optimization technique relies on a representation of the geometry through *level sets*: the device boundary is defined as the zero-level contour of a higher-dimensional scalar function [52].

For topology optimization problems, the number of design variables can easily reach thousands and even millions for 2D and 3D design problems [53, 54]. The large number of design variables means that gradient-based optimization techniques are in practice needed to solve such problems. A main reason for this choice is that the gradient of the objective function contains a massive amount of information, and gradients can in many cases be very efficiently computed by using solutions of associated adjoint-field problems, as discussed in Paper V. To use gradient-based optimization techniques, the design variables are required to vary continuously between the extreme values (that is, requires $p_i \in [0, 1]$ for all i). However, the appearance of intermediate values (values that are neither 0 nor 1, also called "gray values") in the final design could lead to ambiguous representation of the obtained design. Techniques such as solid isotropic material with penalization (SIMP) [45] or artificial damping [55] can be used to suppress these intermediate values in the final design. In contrast, in this thesis the intermediate values of the design variables are strongly self-penalized through the optimization problem formulation itself, and techniques are proposed to *promote* intermediate values during the optimization process.

Topology optimization techniques have been used to design electromagnetic devices by optimizing permittivity or permeability distributions. For example, topology optimization have been used to design magnetic devices by Dyck et al. [32, 33], to design dielectric substrates for bandwidth improvement of patch antennas by Kiziltas et al. [36], and to design dielectric resonator antennas to operate with enhanced bandwidth by Nomura et al. [37]. Recently, topology optimization using the material distribution approach has been used to design metallic devices by Erentok and Sigmund [39], where they reported some difficulties in the interpolation of the conductivity between a good dielectric and a good conductor. To mitigate the interpolation issue in material distribution problems solved by the finite-element method, Aage et al. [27] proposed an implicit impedance boundary condition, which is also used by Nomura et al. [31]. Topology optimization of metallic devices has also been recently addressed by Zhou et al. [38] and Yamasaki et al. [56], using level set methods. The previous contributions to topology optimization of metallic devices, mentioned above, relied on frequency domain methods, and will therefore be efficient only for the optimization of devices operating over a narrow frequency band.

1.7 Finite-difference time-domain method (FDTD)

In his 1966 seminal paper [57], Yee introduced a time-domain numerical technique for the solution of the Maxwell's equations in first-order form. The algorithm was based on a central-difference approximation of Maxwell's equations, with staggered grids for the electric and magnetic fields, solved alternatively at each time step in a leap-frog manner. All implementations of the FDTD method at that time suffered from limitations with respect to the termination of unbounded simulation domains. Mur [58] introduced a stable second-order accurate absorbing boundary condition for the FDTD method. Then, the perfectly matched layer (PML) was introduced by Berenger [59], which solved many of the previously problematic issues with domain termination. Various variants of Berenger's PML have been proposed either to ease the numerical implementation or to account for the absorption of evanescent waves [60, 61].

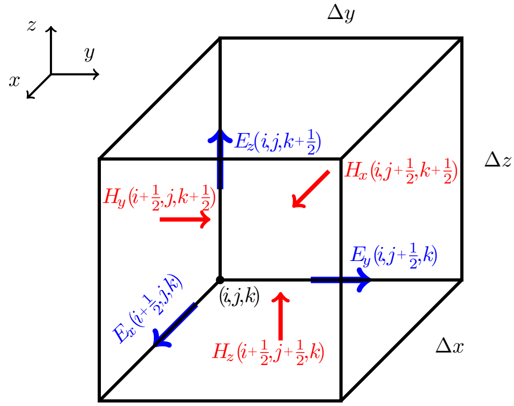

Figure 4: The distribution of the electric and magnetic fields in the basic Yee cell.

Currently, the FDTD method has firmly established itself as one of the most popular methods in computational electromagnetics. Its popularity is mainly due to:

- The ease of implementation.
- The efficiency in terms of low memory footprint due to the explicit time stepping.
- The wide availability of inexpensive and powerful computing resources such as the graphics processing units (GPUs).
- The increasing interest of modeling inhomogeneous materials.
- The wideband data that are potentially available from one simulation.

The FDTD method divides the computational domain into small cubical cells. For each cell, the six field components are located to match the curl operator. Figure 4 shows Yee's cell for a cube (i, j, k) with dimension Δx, Δy, and Δz. The electric field components are located centered and parallel to the cell edges, while the magnetic field components are located centered and normal to the cell faces. Objects are typically represented explicitly in the Yee grid by their constitutive parameters. The conductivity and the permittivity have the same spatial distribution as the discretized electric field, and the permeability has the spatial distribution of the discretized magnetic field. The staggered electric and magnetic grids give uncertainty about the actual boundary of objects in the Yee grid, and simulated objects typically have mesh-dependent effective size [62]. More details about the FDTD method can be found in standard text books [63–65].

Besides being only a second-order-accurate method, a main drawback with the FDTD method is the need to use fine grids to accurately model curved objects and small geometrical features. This is due to the Cartesian grid, which leads to a staircase approximation of any geometry inside the analysis domain. There are several suggested remedies to circumvent the effects of the errors introduced by the staircase approximations, but all generally involve

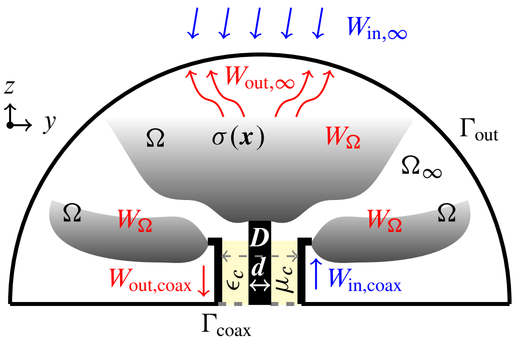

Figure 5: An illustration of the design problem formulation.

additional arithmetic operations at the boundary cells and sometimes cause instabilities. Generally, the material distribution approach to topology optimization a priori requires the design domain to be discretized using fine uniform grids to describe the details of the geometry. This requirement may leave out the main drawbacks of the FDTD method when it is used with topology optimization techniques, since the grid size usually need to be small.

2 Thesis summary

This thesis introduces a gradient-based topology optimization approach to design metallic electromagnetic devices. The focus is to apply the approach to optimize antennas and waveguide transitions; however, the approach can be tailored to design various other electromagnetic devices as well.

2.1 Basic problem setup

The basic problem setup is schematically shown in Figure 5. A design domain Ω holds a conductivity distribution $\sigma(\boldsymbol{x})$ that defines the conductive parts of a device of unknown topology, with $\boldsymbol{x}$ representing a point in the design domain. The device could be an antenna or a waveguide transition, depending on whether the analysis domain $\Omega_\infty \supset \Omega$ is an open space or a waveguide, respectively. A coaxial transmission line couples signals, through an aperture in the xy plane, to and from the analysis domain. The boundary Γ_{coax} is used to introduce wave energy $W_{\text{in,coax}}$ into the coaxial cable, and to measure the wave energy $W_{\text{out,coax}}$ leaving the analysis domain through the coaxial cable. The coaxial cable has an inner core with diameter d, a metallic shield with diameter D, and is filled with a material with dielectric constant ϵ_{c} and permeability μ_{c}. Wave energies $W_{\text{in},\infty}$ and $W_{\text{out},\infty}$, as illustrated in Figure 5, might enter or leave the analysis domain, respectively, through the boundary Γ_{out}.

Inside the analysis domain, assuming no sources inside Ω_∞, the 3D Maxwell's equations govern the relation between the electric field $\boldsymbol{E}$ and the magnetic field $\boldsymbol{H}$,

$$\frac{\partial}{\partial t}\mu \boldsymbol{H} + \nabla \times \boldsymbol{E} = \boldsymbol{0}, \tag{5a}$$

$$\frac{\partial}{\partial t}\epsilon \boldsymbol{E} + \sigma \boldsymbol{E} - \nabla \times \boldsymbol{H} = \boldsymbol{0}. \tag{5b}$$

Inside the lossless coaxial cable, under the assumption that only the TEM mode is supported, the following 1D transport equation is satisfied (PaperII),

$$\frac{\partial}{\partial t}(V \pm Z_c I) \pm c\frac{\partial}{\partial z}(V \pm Z_c I) = 0, \tag{6}$$

where V, I, $c = 1/\sqrt{\mu_c \epsilon_c}$, and Z_c are the potential difference, the current, the phase velocity, and the characteristic impedance of the coaxial cable, respectively. The two terms $V + Z_c I$ and $V - Z_c I$ constitute two signals travelling inside the coaxial cable in the positive and negative z directions, respectively.

Supplied with appropriate initial and boundary conditions, equations (5a), (5b), and (6) can be solved for the electric field $\boldsymbol{E}$, the magnetic field $\boldsymbol{H}$, the current I, and the potential difference V.

2.2 Energy balance and optimization problem

As discussed in Paper II, the initial-boundary-value problem associated with the above setup can be used to derive the energy balance

$$W_{\text{in,coax}} + W_{\text{in},\infty} = W_\Omega + W_{\text{out,coax}} + W_{\text{out},\infty}, \tag{7}$$

in which, as illustrated in Figure 5, the incoming energy $W_{\text{in,coax}} + W_{\text{in},\infty}$ from the coaxial cable and exterior waves equals the total outgoing energy, which comprises the ohmic losses W_Ω in design domain Ω, the outgoing energy $W_{\text{out,coax}}$ through the coaxial cable, and the wave energy $W_{\text{out},\infty}$ exiting through the boundary Γ_{out}.

We note that there are two alternatives to supply incoming energy to the analysis domain, either by $W_{\text{in,coax}}$ through the coaxial cable or by $W_{\text{in},\infty}$ through the boundary Γ_{out}. If the coaxial cable supplies $W_{\text{in,coax}}$, an optimization problem can conceptually be formulated with the objective to maximize the outgoing energy $W_{\text{out},\infty}$. That is, the device is then optimized based on its *transmitting mode*. Note that from energy balance (7), the maximization of $W_{\text{out},\infty}$ implies the minimization of the sum of the two terms $W_{\text{out,coax}}$ and W_Ω (This also implies the minimization of the reflection coefficient inside the coaxial cable plus the maximization of the radiation efficiency (cf. Sec. 1.2)). On the other hand, if the boundary Γ_{out} is used to supply incoming energy $W_{\text{in},\infty}$, we may conceptually formulate an optimization problem with the objective to maximize the outgoing energy $W_{\text{out,coax}}$ through the coaxial cable. That is, the device is then optimized based on its *receiving mode*. Note also that by energy balance (7), the maximization of $W_{\text{out,coax}}$ implies the minimization of the sum of the two terms $W_{\text{out},\infty}$ and W_Ω.

Both formulations thus tend to minimize the losses in order to maximize the corresponding objective function.

The second alternative is computationally more efficient when time-domain numerical methods are used, since the full-time history of the observed signal is needed to efficiently compute the gradient of the objective function by adjoint-field methods, as described in Paper V. Observation of the outgoing signal in the coaxial cable requires less memory than observation of the outgoing waves $W_{\text{out},\infty}$. Therefore, the second choice is adopted to formulate the conceptual optimization problem

$$\begin{aligned} \max_{\sigma(\boldsymbol{x})\in[\sigma_{\min},\sigma_{\max}]} \quad & W_{\text{out,coax}}\left(\sigma\left(\boldsymbol{x}\right)\right), \\ \text{s.t.} \quad & \text{the governing equations}, \\ & \text{exterior wave sources}\left(W_{\text{in},\infty}\right), \\ & W_{\text{in,coax}} = 0, \end{aligned} \tag{8}$$

where $\sigma_{\min}$ and $\sigma_{\max}$ represent physical conductivities of a low-loss dielectric and a good conductor, respectively. The outgoing energy in the coaxial cable can be computed, using the signal $V - Z_{\text{c}} I$ in expression (6), as follow

$$W_{\text{out,coax}} = \frac{1}{4Z_{\text{c}}} \int_0^T \left(V - Z_{\text{c}} I\right)^2 dt, \tag{9}$$

where T denotes the length of the observation time interval.

2.3 Numerical treatment

The FDTD method is used to numerically solve the time-domain Maxwell's equations with the open space radiation condition simulated using a uniaxial perfectly matched layer (UPML) [60, 61]. The design variables are the conductivity value at each Yee edge i in the design domain Ω.

Let $\boldsymbol{\sigma}$ be a vector that holds the conductivity components at each Yee edge inside the domain Ω. We introduce the normalized density vector $\boldsymbol{p}$, whose components are mapped to the physical conductivities through

$$\sigma_{\text{i}} = 10^{(c_1 p_{\text{i}} - c_2)} \quad \text{S/m}, \tag{10}$$

where the scalars c_1 and c_2 are selected to control the physical conductivity range $[\sigma_{\min}, \sigma_{\max}]$. In the numerical experiments in this thesis, we observed a very low sensitivity in the objective function to variations in conductivities below $\sigma_{\min} = 10^{-4}$ S/m or above $\sigma_{\max} = 10^5$ S/m. Therefore, we usually use expression (10) with $c_1 = 9$ and $c_2 = 4$.

Based on the FDTD method, a discrete version of optimization problem (8) can be written as

$$\begin{aligned} \max_{\boldsymbol{p}} \quad & W^{\Delta}_{\text{out,coax}}\left(\boldsymbol{p}\right), \\ \text{s.t.} \quad & \text{the discretized governing equations}, \\ & \text{exterior wave sources}\left(W^{\Delta}_{\text{in},\infty}\right), \\ & W^{\Delta}_{\text{in,coax}} = 0, \end{aligned} \tag{11}$$

with the discrete objective function defined as

$$W^{\Delta}_{\text{out,coax}}(\boldsymbol{p}) = \frac{1}{Z_m} \sum_{n=0}^{N} (V^{n+1} - \hat{Z}_{\text{c}} I_z^{n+\frac{1}{2}})^2 \, \Delta t, \tag{12}$$

where V^{n+1}, $I_z^{n+\frac{1}{2}}$, and $\hat{Z}_{\text{c}}$ are the potential difference, the current, and the characteristic impedance of the discrete coaxial cable model proposed in Paper II; $Z_{\text{m}} = \sqrt{\mu_c/\epsilon_c}$; N is the total number of time steps used in the simulation; and Δt is the time step used in the FDTD method. An efficient technique to implement the exterior wave sources $W^{\Delta}_{\text{in},\infty}$ in the FDTD method is to use the total-field scattered-field formulation [63]. To control the frequency spectrum of the incoming waves, throughout this thesis, we used a time-domain truncated *sinc* signal that is usually modulated to the center of the frequency band of interest [66].

To solve optimization problem (11) by a gradient-based optimization algorithm, the gradient of the objective function (12) is required. In Paper V, the adjoint-field method and the FDTD discretization of Maxwell's equations are used to derive the following expression for the gradient of objective function (12),

$$\frac{\partial W^{\Delta}_{\text{out,coax}}}{\partial \sigma_i} = -\Delta^3 \sum_{n=1}^{N} E_i^{N-n} \frac{E_i^{*\,n-\frac{1}{2}} + E_i^{*\,n+\frac{1}{2}}}{2} \, \Delta t, \tag{13}$$

where i denotes the index of an arbitrary Yee-edge inside the design domain; Δ is the spatial discretization step; E_i is the discrete electric field obtained from the FDTD solution to equations (5) and (6); and E_i^* is a discrete adjoint electric field obtained by solving an adjoint-field problem. The adjoint-field problem is similar to the FDTD discretization of equations (5), except that the adjoint-field problem is excited through the boundary Γ_{coax}, at the bottom of the coaxial cable, using the expression

$$V^{*\,n-\frac{1}{2}} + \hat{Z}_{\text{c}} I_z^{*\,n-1} = V^{N-n+1} - \hat{Z}_{\text{c}} I_z^{N-n+\frac{1}{2}} \quad \text{for } n = 1, \dots, N, \tag{14}$$

where $V^{*\,n-\frac{1}{2}}$ and $I_z^{*\,n-1}$ are the discrete potential difference and the current inside the coaxial cable of the adjoint problem. Note that the left side of expression (14) constitutes a signal propagating inside the coaxial cable in the positive z direction, and that the right side is the time-reversed signal that propagates in the negative z direction for the original-field problem. In other words, the time-reversed received signal in the original-field problem constitutes the incoming signal for the adjoint-field problem.

Thus, by using two FDTD solutions, the objective function and the gradient vector can be computed for *any* number of design variables inside the design domain Ω. In this thesis, the globally convergent method of moving asymptotes (GCMMA) [67] is used to update the design variables. The GCMMA is a first-order gradient-based optimization method that belong to the class of sequential convex approximation methods [17, ch4].

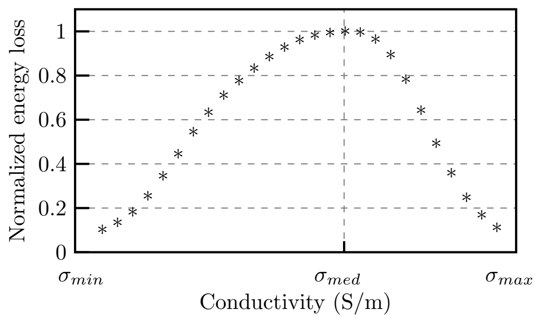

Figure 6: The energy loss versus the value of the design domain conductivity. Typical values for $\sigma_{\text{min}} = 10^{-2}$ S/m, $\sigma_{\text{med}} = 10^{2}$ S/m, and $\sigma_{\text{max}} = 10^{5}$ S/m.

2.4 Self-Penalization

Problem (11) is strongly *self-penalized* towards the lossless design cases. More precisely, solving problem (11) by gradient-based optimization methods leads, after only a few iterations, to designs consisting mainly of a good conductor (σ_{max}) or a good dielectric (σ_{min}). The reason for the strong self-penalization can be explained, using energy balance (7), as follows. For a given incoming energy $W_{\text{in},\infty}$, to maximize the outgoing energy, $W_{\text{out,coax}}$, the energy losses, W_{Ω}, inside the design domain should by minimized. The intermediate conductivities contribute to higher energy losses than the extreme conductivities, as illustrated in Figure 6. Thus, any gradient-based optimization method will attempt to minimize the energy losses, W_{Ω}, by moving the edge conductivities towards the lossless case (σ_{min} or σ_{max}). Unfortunately, the resulting optimized designs often consist of scattered metallic parts and exhibit bad performance, as demonstrated in Paper III.

To relax the self-penalization, we use a filtering approach, proposed in Paper I. The goal of the filtering is to promote intermediate conductivities inside the design domain during the initial phase of the optimization to counteract the self-penalization. To do so, we replace $\boldsymbol{p}$ by $\tilde{\boldsymbol{p}} = \boldsymbol{K}\,\boldsymbol{p}$ in expression (10). The filter matrix $\boldsymbol{K}$ approximates an integral operator with support over a disc with radius R. By using the filter, each component in the vector $\boldsymbol{p}$ is replaced by a weighted average of the neighboring components, where the weights vary linearly from a maximum value at the center of the disc to zero at the perimeter. The filter effectively blurs the design variables $\boldsymbol{p}$ and thus impose intermediate conductivities inside the design domain Ω. However, to avoid having losses in the final design, the optimization problem is solved following a continuation approach. Starting with initial radius R_0, optimization problem (11) is solved for a sequence of subproblems, where after partial convergence of a subproblem, the filter radius is reduced by setting $R_{n+1} = \gamma R_n$, where $\gamma < 1$ is a constant filter decrease coefficient. The convergence of a subproblem is evaluated based on the change of the norm of the first-order optimality conditions. The algorithm terminates when the radius R_n decreases beyond a small value, typically chosen to be smaller than the numerical grid size Δ. Typically, the final design consists essentially of two conductivity values that correspond to σ_{min} and σ_{max}.

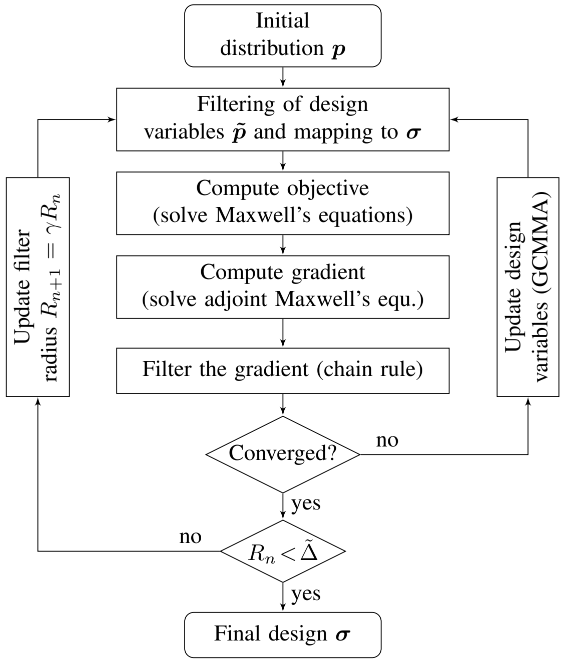

Figure 7: A flowchart of the optimization process.

2.5 Summary of the optimization process

The flowchart in Figure 7 illustrates the optimization process. The process starts with a uniform initial distribution of the design variables, $\boldsymbol{p}$, which typically corresponds to a conductivity around the peak in Figure 6. Starting with an initial filter radius R_0, the optimization problem is solved through solutions to a number of subproblems. In each subproblem, the design variables are filtered and mapped to the physical conductivities $\boldsymbol{\sigma}$. Then the FDTD method numerically solves Maxwell's equations and the associated adjoint-field problem in order to compute the objective function and the gradient vector. The chain rule is used to obtain the gradient with respect to the design variables $\boldsymbol{p}$. Then a convergence criterion based on the first-order necessary condition is tested. If the convergence criterion is not satisfied, the optimization process continues to a new cycle in the current subproblem, where the GCMMA algorithm use the gradient and the objective function values to update the design variables. The GCMMA might evaluate the objective function a few additional times to find updates that satisfy a sufficient improvement condition of the objective function. If the convergence criterion is reached but the filter radius is greater than $\tilde{\Delta} = \Delta/\sqrt{2}$, the minimal distance between two conductivity components in the Yee grid, the radius of the filter is reduced, $R_{n+1} = \gamma R_n$, and a new subproblem starts. Finally, the optimization process terminates if the convergence criterion is satisfied and the filter radius is smaller than or equal to $\tilde{\Delta}$. Typically, the optimized design consists of conductivities that are either $\sigma_{\min}$ or $\sigma_{\max}$. In a

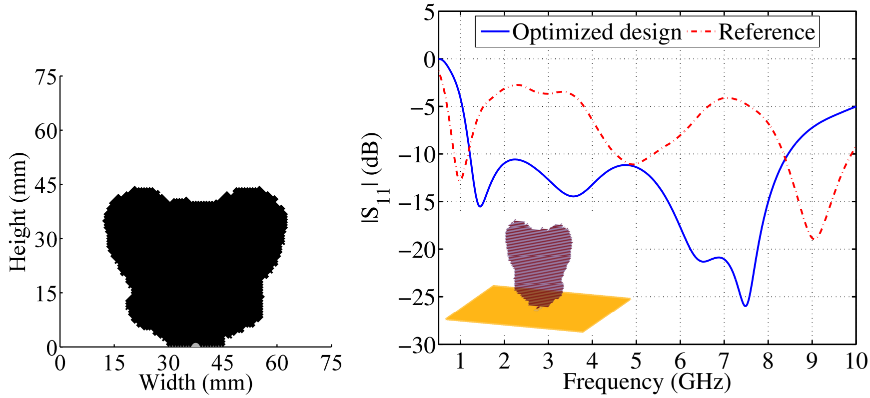

Figure 8: Left: the final conductivity distribution of the monopole designed based on linearly-polarized plane wave excitation. The optimization problem has $20,200$ design variables (the coaxial cable connection point is marked by a gray dot). Right: the reflection coefficient of the antenna.

final step before evaluating the performance of the optimized design, a threshold conductivity $\sigma_{\text{th}} = 0.1$ S/m is usually used to map conductivities below and above σ_{th} to 0 S/m (void) and 5.8×10^7 S/m (copper), respectively.

2.6 Selected results

2.6.1 Ultrawideband (UWB) monopole design

Recently, UWB antennas have received great attention in applications such as wireless communication and high resolution radar [68, 69]. A key candidate for UWB antennas is the planar monopole. In Paper I, optimization problem (11) is used for the complete layout optimization of the radiating element of planar monopole antennas. We use a design domain that has an area of 75×75 mm^2, located 0.75 mm above a simulated infinite ground plane, and connected at the center of its bottom side to a 50 Ω coaxial cable. The design domain is discretized into 100×100 Yee cell faces, which yields $20,200$ design variables (one conductivity component for each Yee edge). The objective is to maximize the energy received by the planar monopole over the frequency band 1–10 GHz.

The analysis domain is excited by a set of external sources that surround the monopole and radiate linearly-polarized plane waves. Figure 8 shows the final design obtained by the optimization algorithm in 132 iterations. The final design uses only around 50×45 mm^2 out of the available design domain area. The reflection coefficient $|S_{11}|$ of the optimized monopole is below -10 dB over the frequency band $1.2 - 8.5$ GHz. Included in the same

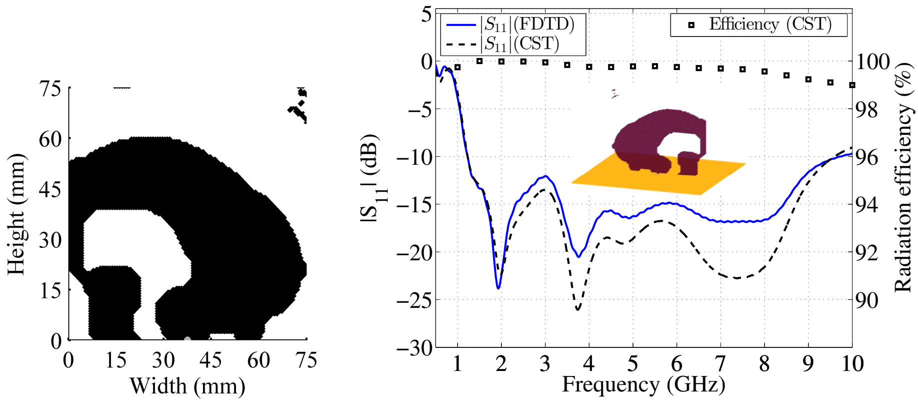

Figure 9: Left: the final conductivity distribution of the monopole designed based on circularly-polarized plane wave excitation. The optimization problem has $20,200$ design variables (the coaxial cable connection point is marked by a gray dot). Right: the reflection coefficient and the radiation efficiency of the antenna.

figure as a reference for comparison, is the reflection coefficient of the planar monopole antenna obtained when the whole design domain area is filled with a perfect conductor.

When the excitation sources are set to radiate essentially circularly-polarized plane waves, the design shown in Figure 9 is obtained by the optimization algorithm in 126 iterations. In this case, the monopole reflection coefficient $|S_{11}|$ is below -10 dB over the frequency band $1.23 - 9.75$ GHz. Included in the same figure for verification purposes, are the reflection coefficient and the radiation efficiency of the antenna computed with the CST Microwave Studio package (https://www.cst.com/).

2.6.2 Microstrip antenna design

Microstrip antennas have been one of the most attractive antennas to use in many wireless systems because of their many unique and attractive properties: low profile, compact and conformable structure, and ease of fabrication and integration with microwave devices [3].

We use optimization problem (11) to design the radiating patch of a microstrip antenna in order to radiate around 1.5 GHz with 0.2 GHz bandwidth. The design domain has the same area and discretization as the UWB monopole case; however, here this domain is used as the radiating patch of a microstrip antenna. The radiating patch is located 6 mm above a simulated infinite ground plane. We use a dielectric substrate with relative permittivity of 2.62 and loss tangent of 0.001 at 2 GHz. The optimization algorithm converged to the final design in 118 iterations. Figure 10 shows the optimized conductivity and the performance of the antenna. Note that the inner probe of the 50 Ω coaxial cable is connected to the radiating patch at (18.75 mm,37.5 mm) and is marked by a gray dot. The CST package is used to

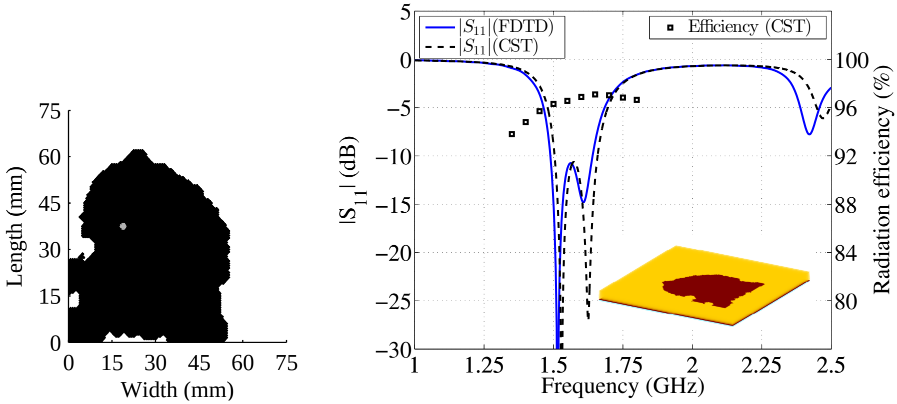

Figure 10: Left: the final conductivity distribution over the patch area of the microstrip antenna optimized to radiate at 1.5 GHz (the probe connection point is marked by a gray dot). Right: the reflection coefficient and the radiation efficiency.

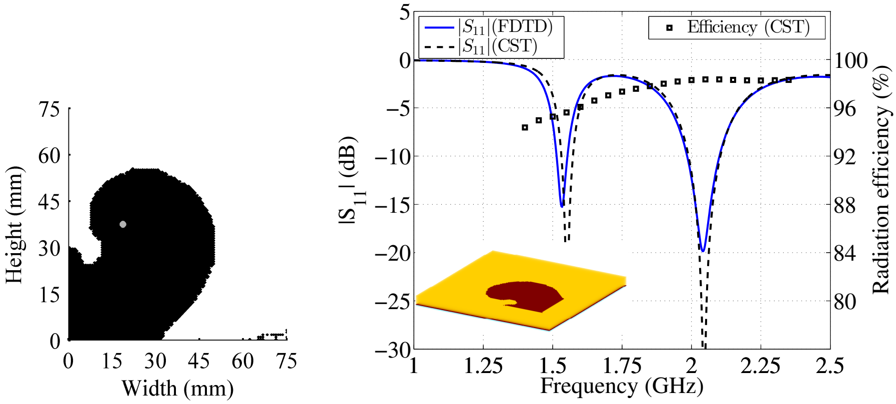

Figure 11: Left: the final conductivity distribution over the patch area of the microstrip antenna that radiates over two frequency bands centered around 1.5 GHz and 2 GHz (the probe connection point is marked by a gray dot). Right: the reflection coefficient and the radiation efficiency.

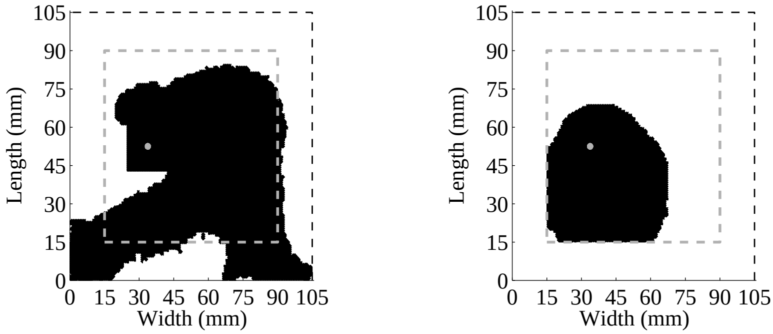

Figure 12: Left: the optimized conductivity distribution over the ground plane when the radiating patch and the ground plane are simultaneously designed. Right: the optimized conductivity over the patch area. The design problem has in total 58,276 design variables (the location of the coaxial probe is marked by a gray dot).

compute the radiation efficiency of the antenna and to cross-verify the reflection coefficient computed by the FDTD method.

The same design domain is used to design a dual-band microstrip antenna, with the two frequency bands centered around 1.5 and 2.0 GHz. The design problem (11) is slightly modified, to account for the energy received from the two bands, as

$$\max_{\boldsymbol{p}} \quad \sum_{i=1}^{2} |W^{(i)}_{\text{out,coax}}(\boldsymbol{p})|^{\frac{1}{2}}. \tag{15}$$

Figure 11 shows the geometry of the antenna, and the computed reflection coefficient and radiation efficiency. The optimization algorithm converged to the final design after 120 iterations.

In the previous two cases, the ground plane of the microstrip antennas is considered electrically large and is simulated as an infinite ground plane. In many realistic situations, microstrip antennas are mounted over a finite ground plane. Generally, the ground plane is considered as a part of the antenna structure and, therefore, affects the antenna radiation, especially when the ground plane size is electrically small. In the literature, the design of the ground plane is usually considered in a separate design phase [70–73], which is typically pursued after the design of the radiating patch of the antenna. In Paper III, a microstrip antenna mounted over a finite ground plane is designed to operate at 1.5 GHz with 0.3 GHz bandwidth. Both the ground plane and the radiating patch are considered in the design. A dramatic improvement in performance is observed when both the radiating patch and the ground plane are simultaneously designed. Figure 12 shows the optimized conductivity distribution over the ground plane (left) and the radiating patch (right). The design problem has in total 58,276 design variables, and the optimization algorithm required 125 iterations. Figure 13 shows the reflection coefficient and the radiation efficiency of the obtained design computed with our FDTD code and cross-verified with the CST package. Figure 14 shows the

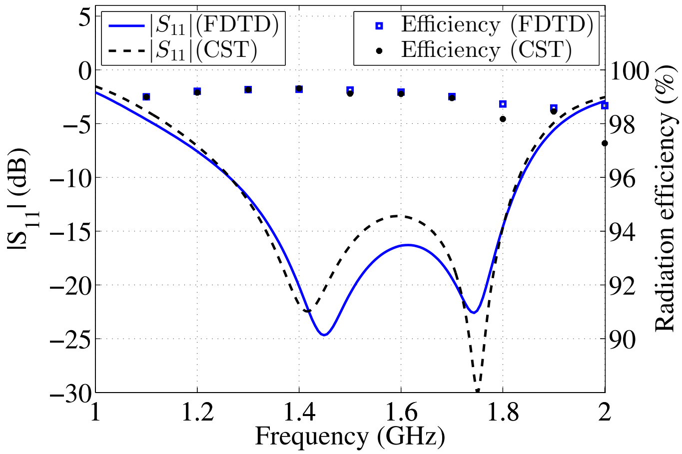

Figure 13: The reflection coefficient and the radiation efficiency of the designs given in Figure 12.

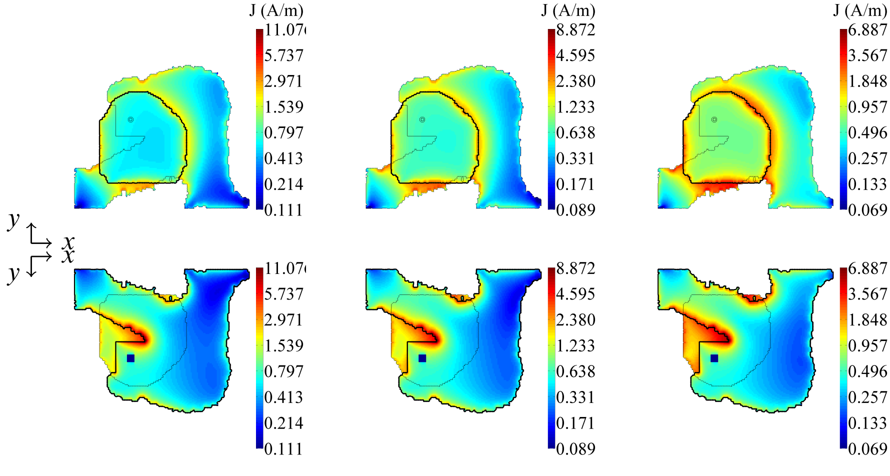

Figure 14: Surface currents over the radiating patch and the ground plane given in Figure 12 at 1.4, 1.5, and 1.6 GHz. The first row is the surface currents seen from the positive z axis, and the second row is the surface currents seen from the negative z axis.

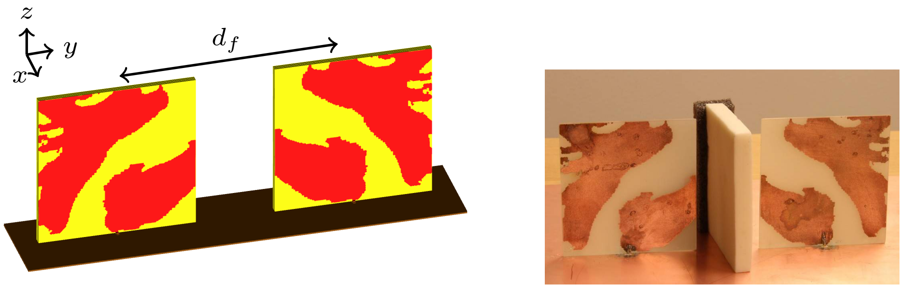

Figure 15: Left: the geometry of the optimized antennas with a feed-to-feed distance $d_f = 116.90$ mm. Right: the manufactured prototype when used to detect a nearby phantom that represents human muscle tissue.

surface current distribution, computed by the FDTD method, at 1.4, 1.5, and 1.6 GHz over the optimized conductive parts of the antenna. The peaks of the surface current (the red color) that occur on the ground plane indicate the essential role of the ground plane in the antenna radiation.

2.6.3 Wideband planar directive antennas

The growing interest of using microwave detection and imaging systems, especially for medical applications, raises more demands on the design of wideband directive antennas. In the literature, there are a few antenna types that are characterized as being wideband as well as directive. The most known directive antenna is the tapered slot antenna, known as the Vivaldi antenna, or its variant the antipodal Vivaldi antenna [74, 75]. A conventional Vivaldi antenna is generally described by a few parameters, which limits the possibility to optimize the antenna structure to achieve a satisfactory performance. Moreover, focusing on enlarging the impedance bandwidth of Vivaldi antennas might reduce the required directivity, especially at the lower frequencies where the antenna arms can radiate as monopole.

In Paper IV, planar directive antennas are designed by formulating an optimization problem with the objective to maximize the coupling between two antennas separated by a specific distance. The frequency band of interest is 1–10 GHz. Figure 15 shows one of the optimized planar antennas. Each antenna has an area of 77.94×77.94 mm^2 and the two antennas are separated a feed-to-feed distance $d_f = 116.90$ mm. The design problem has $39,480$ design variables and the optimization algorithm required 188 iterations to converge to the final design shown to the left in Figure 15. Figure 15 shows also the manufactured antennas. Fig. 16 shows the coupling coefficient, $|S_{21}|$, and the reflection coefficient, $|S_{11}|$, of the antennas, evaluated experimentally and through simulations by the FDTD method and the CST package. In order to evaluate their performance, the optimized antennas are used to detect a phantom that represents human muscle tissue. We study the detection sensitivity, measured as the difference

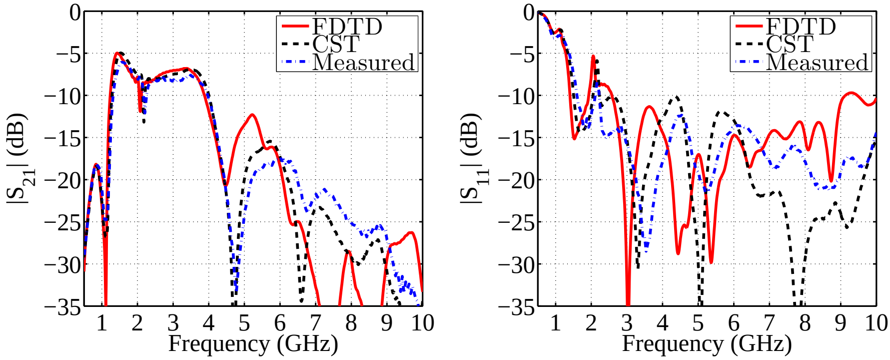

Figure 16: Left: the coupling coefficient between the two monopoles given in Figure 15. Right: the reflection coefficient.

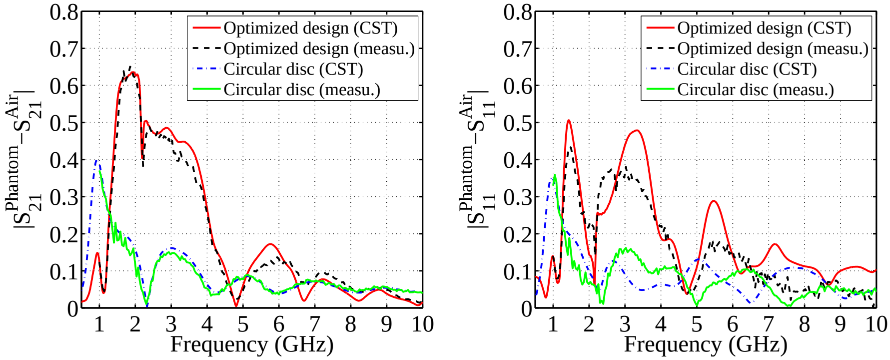

Figure 17: Left: the difference between the coupling coefficients in presence and absence of 80×80×10 mm^3 phantom, for the optimized antennas in Figure 15 and for an UWB disc monopole antennas with comparable size. Right: the difference in the reflection coefficients.

in the scattering parameters between the cases presence and absence of the phantom. That is, we compute ($|S_{ij}^{\text{Phantom}} - S_{ij}^{\text{Air}}|$) for $i, j = 1, 2$. Figure 17 shows the detection sensitivities of the optimized antennas compared to the detection sensitivities of a pair of UWB disc monopole antennas, when both are used to detect the same phantom. As can be seen from Figure 17, the optimized antennas give more than 300% improvement in signal strength over a wide frequency band, compared to the reference UWB disc monopoles.

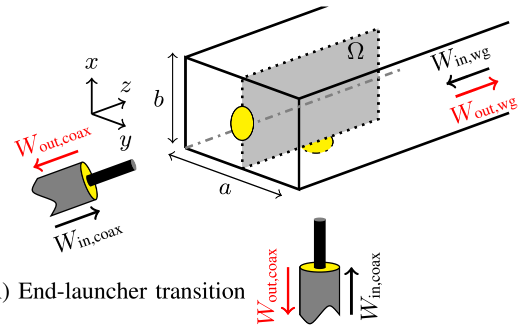

(A) End-launcher transition

(B) Right-angle transition

Figure 18: Optimizing the conductivity over the design domain Ω (the gray region enclosed by the dotted line) to match the 50 Ohm coaxial cable (A or B) to a standard rectangle waveguide with cross section $a \times b$.

2.6.4 Waveguide transitions

At transition planes, where a transmission line is connected to a device or to a different transmission line, a mismatch between the two sides reduces the system efficiency. The mismatch problem is more prominent for systems operating over wide frequency bands, since microwave components typically have frequency dependent characteristics. Many wideband coaxial-to-waveguide transitions have been reported in the literature [76–78]. However, most of the proposed transitions still depend essentially on the concept of cascading various transmission line sections, with only few parameters to optimize. Besides requiring much space to install, the complexity of assembling various sections, especially when 3D structures are involved, can hinder mass production of such transitions.

We use optimization problem (11) to design transitions between standard rectangular waveguides and a 50 Ohm coaxial cable. We consider the design of two types of transitions, right-angle transitions and end-launcher transitions, illustrated in Figure 18. Here, the analysis domain Ω_∞ is bounded from five sides by the waveguide walls and extends to infinity in the sixth direction (positive z). The design domain Ω is backed by an RT/Duroid 5880 LZ substrate (ϵ_r = 1.96, thickness = 1.27 mm) to support the conducting patches. Figure 19 shows the geometry and the performance for one of the optimized right-angle transitions. The optimization problem has 28, 410 design variables and is solved by the design algorithm in 226 iterations. The reflection and the coupling coefficients of the transition are shown in Figure 19, with the coaxial cable designated as port 1 and the waveguide as port 2. There is good match between the experimental results and the results computed by the FDTD method and the CST package. The two vertical dotted lines determine the targeted frequency band, for which the transition is optimized. The transition has a reflection coefficient lower than -10 dB over the frequency band 6.75–13.5 GHz (66% bandwidth) and a corresponding coupling coefficient higher than -0.5 dB. Figure 20 shows the fabricated prototype.

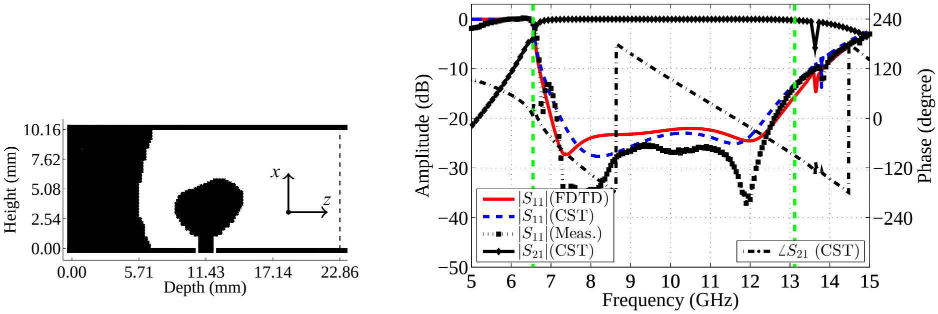

Figure 19: Left: the optimized conductivity distribution enclosed by three of the waveguide walls and the dashed line. Right: the scattering parameters of the right-angle transition.

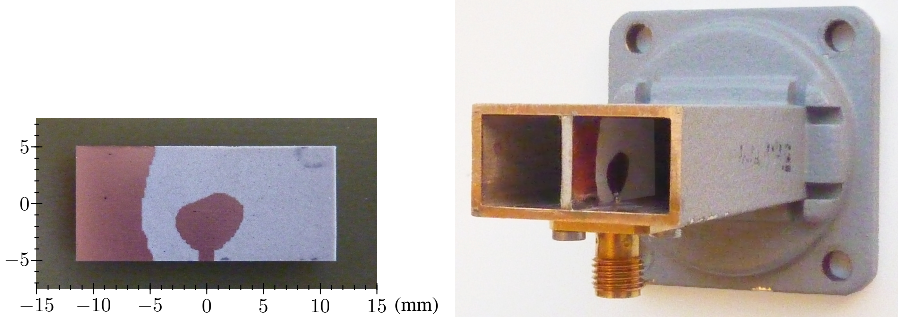

Figure 20: Left: the fabricated prototype of the optimized design backed by the RT/Duroid 5880 LZ substrate. Right: the assembled right-angle transition (the shorting wall at $z = 0$ is removed for visibility).

References

[1] *IEEE Standard for Definitions of Terms for Antennas*, IEEE Std 145-2013, 2014.

[2] C. A. Balanis, *Advanced Engineering Electromagnetics*. John Wiley & Sons, 1989.

[3] ——, *Antenna Theory: Analysis and Design*, 3rd ed. Wiley-Interscience, 2005.

[4] M. N. Sadiku, *Numerical Techniques in Electromagnetics*, 2nd ed. CRC Press, 2001.

[5] J. Zhu, J. Bandler, N. Nikolova, and S. Koziel, "Antenna optimization through space mapping," *IEEE Trans. Antennas Propag.*, vol. 55, no. 3, pp. 651–658, March 2007.

[6] S. Koziel, S. Ogurtsov, J. Bandler, and Q. Cheng, "Reliable space-mapping optimization integrated with EM-based adjoint sensitivities," *IEEE Trans. Microw. Theory Tech.*, vol. 61, no. 10, pp. 3493–3502, Oct 2013.

[7] K. Sörensen, "Metaheuristics–the metaphor exposed," *Int. Trans. in Op. Res.*, vol. 22, no. 1, pp. 3–18, 2015.

[8] R. L. Haupt, "An introduction to genetic algorithms for electromagnetics," *IEEE Antennas Propag. Mag.*, vol. 37, no. 2, pp. 7–15, 1995.

[9] J. Robinson and Y. Rahmat-Samii, "Particle swarm optimization in electromagnetics," *IEEE Trans. Antennas Propag.*, vol. 52, no. 2, pp. 397–407, Feb 2004.

[10] S. Kirkpatrick, C. D. Gelatt, and M. P. Vecchi, "Optimization by simulated annealing," *Science*, vol. 220, no. 4598, pp. 671–680, 1983.

[11] J. Perez and J. Basterrechea, "Comparison of different heuristic optimization methods for near-field antenna measurements," *IEEE Trans. Antennas Propag.*, vol. 55, no. 3, pp. 549 –555, Mar. 2007.

[12] M. John and M. Ammann, "Wideband printed monopole design using a genetic algorithm," *IEEE Antennas Wireless Propag. Lett.*, vol. 6, pp. 447 –449, 2007.

[13] L. Griffiths, C. Furse, and Y. C. Chung, "Broadband and multiband antenna design using the genetic algorithm to create amorphous shapes using ellipses," *IEEE Trans. Antennas Propag.*, vol. 54, no. 10, pp. 2776 –2782, Oct. 2006.

[14] F. Villegas, T. Cwik, Y. Rahmat-Samii, and M. Manteghi, "A parallel electromagnetic genetic-algorithm optimization (EGO) application for patch antenna design," *IEEE Trans. Antennas Propag.*, vol. 52, no. 9, pp. 2424 – 2435, Sep. 2004.

[15] O. Sigmund, "On the usefulness of non-gradient approaches in topology optimization," *Struct. Multidiscip. Optim.*, vol. 43, pp. 589–596, 2011.

[16] J. Nocedal and S. Wright, *Numerical optimization*. Springer-Verlag New York, 1999.

[17] P. Christensen and A. Klarbring, *An Introduction to Structural Optimization*. Springer Netherlands, 2008.

[18] M. Gustafsson and S. He, “An optimization approach to two-dimensional time domain electromagnetic inverse problems,” *Radio Science*, vol. 35, no. 2, pp. 525–536, Mar. 2000.

[19] Y.-S. Chung, C. Cheon, and S.-Y. Hahn, “Reconstruction of dielectric cylinders using FDTD and topology optimization technique,” *IEEE Trans. Magn.*, vol. 36, no. 4, pp. 956–959, Jul 2000.

[20] Y.-S. Chung, C. Cheon, I.-H. Park, and S.-Y. Hahn, “Optimal design method for microwave device using time domain method and design sensitivity analysis. II. FDTD case,” *IEEE Trans. Magn.*, vol. 37, no. 5, pp. 3255 –3259, Sep. 2001.

[21] I. Rekanos, “Inverse scattering in the time domain: an iterative method using an FDTD sensitivity analysis scheme,” *IEEE Trans. Magn.*, vol. 38, no. 2, pp. 1117–1120, Mar 2002.

[22] E. Abenius and B. Strand, “Solving inverse electromagnetic problems using FDTD and gradient-based minimization,” *Int. J. Num. Meth. Eng.*, vol. 68, no. 6, pp. 650–673, 2006.

[23] P. Jacobsson and T. Rylander, “Gradient-based shape optimisation of conformal array antennas,” *IET Microw. Antennas Propag.*, vol. 4, no. 2, pp. 200–209, Feb. 2010.

[24] N. Nikolova, H. Tam, and M. Bakr, “Sensitivity analysis with the FDTD method on structured grids,” *IEEE Trans. Microw. Theory Tech.*, vol. 52, no. 4, pp. 1207 – 1216, Apr. 2004.

[25] A. Bondeson, Y. Yang, and P. Weinerfelt, “Shape optimization for radar cross sections by a gradient method,” *Int. J. Num. Meth. Eng.*, vol. 61, no. 5, pp. 687–715, 2004.

[26] M. H. Bakr, O. S. Ahmed, M. H. E. Sherif, and T. Nomura, “Time domain adjoint sensitivity analysis of electromagnetic problems with nonlinear media,” *Opt. Express*, vol. 22, no. 9, pp. 10 831–10 843, May 2014.

[27] N. Aage, N. A. Mortensen, and O. Sigmund, “Topology optimization of metallic devices for microwave applications,” *Int. J. Num. Meth. Eng.*, vol. 83, no. 2, pp. 228–248, 2010.

[28] A. Diaz and O. Sigmund, “A topology optimization method for design of negative permeability metamaterials,” *Struct. Multidiscip. Optim.*, vol. 41, pp. 163–177, 2010.

[29] H. Khalil, A. Assadihaghi, S. Bila, D. Baillargeat, M. Aubourg, S. Verdeyme, J. Puech, and L. Lapierre, “Topology gradient optimization in 2-D and 3-D for the design of microwave components,” *Microw. Opt. Technol. Lett.*, vol. 50, no. 10, pp. 2739–2743, 2008.

[30] S. Koziel, F. Mosler, S. Reitzinger, and P. Thoma, “Robust microwave design optimization using adjoint sensitivity and trust regions,” *Int. J. Rf. Microw. C. E.*, vol. 22, no. 1, pp. 10–19, 2012.

[31] T. Nomura, M. Ohkado, P. Schmalenberg, J. Lee, O. Ahmed, and M. Bakr, “Topology optimization method for microstrips using boundary condition representation and adjoint analysis,” in *EuMC2013*, Oct 2013, pp. 632–635.

[32] D. Dyck, D. Lowther, and E. Freeman, “A method of computing the sensitivity of electromagnetic quantities to changes in materials and sources,” *IEEE Trans. Magn.*, vol. 30, no. 5, pp. 3415 –3418, Sep. 1994.

[33] D. Dyck and D. Lowther, “Automated design of magnetic devices by optimizing material distribution,” *IEEE Trans. Magn.*, vol. 32, no. 3, pp. 1188 –1193, May 1996.

[34] T. Labbé and B. Dehez, “Convexity-oriented method for the topology optimization of ferromagnetic moving parts in electromagnetic actuators using magnetic energy,” *IEEE Trans. Magn.*, vol. 46, no. 12, pp. 4016–4022, Dec 2010.

[35] M. Otomori, T. Yamada, K. Izui, S. Nishiwaki, and N. Kogiso, “Level set-based topology optimization for the design of a ferromagnetic waveguide,” *IEEE Trans. Magn.*, vol. 48, no. 11, pp. 3072–3075, Nov 2012.

[36] G. Kiziltas, D. Psychoudakis, J. Volakis, and N. Kikuchi, “Topology design optimization of dielectric substrates for bandwidth improvement of a patch antenna,” *IEEE Trans. Antennas Propag.*, vol. 51, no. 10, pp. 2732 – 2743, Oct. 2003.

[37] T. Nomura, K. Sato, K. Taguchi, T. Kashiwa, and S. Nishiwaki, “Structural topology optimization for the design of broadband dielectric resonator antennas using the finite difference time domain technique,” *Int. J. Num. Meth. Eng.*, vol. 71, pp. 1261–1296, 2007.

[38] S. Zhou, W. Li, and Q. Li, “Level-set based topology optimization for electromagnetic dipole antenna design,” *J. Comput. Phys.*, vol. 229, no. 19, pp. 6915 – 6930, 2010.

[39] A. Erentok and O. Sigmund, “Topology optimization of sub-wavelength antennas,” *IEEE Trans. Antennas Propag.*, vol. 59, no. 1, pp. 58 –69, Jan. 2011.

[40] M. Ghassemi, M. Bakr, and N. Sangary, “Antenna design exploiting adjoint sensitivity-based geometry evolution,” *IET Microw. Antennas Propag.*, vol. 7, no. 4, pp. 268–276, Mar. 2013.

[41] P. Jacobsson and T. Rylander, “Shape optimization of the total scattering cross section for cylindrical scatterers,” *Radio Science*, vol. 44, no. 4, Aug. 2009.

[42] N. Uchida, S. Nishiwaki, K. Izui, M. Yoshimura, T. Nomura, and K. Sato, “Simultaneous shape and topology optimization for the design of patch antennas,” in *EuCAP 2009*, Mar. 2009, pp. 103–107.

[43] J. Kataja, S. Jarvenpää, J. Toivanen, R. Mäkinen, and P. Ylä-Oijala, "Shape sensitivity analysis and gradient-based optimization of large structures using MLFMA," *IEEE Trans. Antennas Propag.*, vol. 62, no. 11, pp. 5610–5618, Nov. 2014.

[44] M. P. Bendsøe and N. Kikuchi, "Generating optimal topologies in structural design using a homogenization method," *Comput. Methods in Appl. Mech. Eng.*, vol. 71, no. 2, pp. 197–224, 1988.

[45] M. P. Bendsøe and O. Sigmund, *Topology Optimization. Theory, Methods, and Applications*. Springer, 2003.

[46] O. Sigmund and K. Maute, "Topology optimization approaches," *Struct. Multidiscip. Optim.*, vol. 48, no. 6, pp. 1031–1055, 2013.

[47] J. Deaton and R. Grandhi, "A survey of structural and multidisciplinary continuum topology optimization: post 2000," *Struct. Multidiscip. Optim.*, vol. 49, no. 1, pp. 1–38, 2014.

[48] E. Wadbro, "Analysis and design of acoustic transition sections for impedance matching and mode conversion," *Struct. Multidiscip. Optim.*, vol. 50, no. 3, pp. 395–408, 2014.

[49] J. Jensen and O. Sigmund, "Topology optimization for nano-photonics," *Laser Photon. Rev.*, vol. 5, no. 2, pp. 308–321, 2011.

[50] Y.-S. Chung, B.-J. Lee, and S.-C. Kim, "Optimal shape design of dielectric micro lens using FDTD and topology optimization," *J. Opt. Soc. Korea*, vol. 13, no. 2, pp. 286–293, Jun. 2009.

[51] J. Andkjær, V. Johansen, K. Friis, and O. Sigmund, "Inverse design of nanostructured surfaces for color effects," *J. Opt. Soc. Am. B*, vol. 31, no. 1, pp. 164–174, 2014.

[52] G. Allaire, F. Jouve, and A.-M. Toader, "A level-set method for shape optimization," *C. R. Acad. Sci. Paris Sér. I Math.*, vol. 334, no. 12, pp. 1125–1130, 2002.

[53] E. Wadbro and M. Berggren, "Megapixel topology optimization on a graphics processing unit," *SIAM Review*, vol. 51, no. 4, pp. 707–721, 2009.

[54] N. Aage and B. Lazarov, "Parallel framework for topology optimization using the method of moving asymptotes," *Struct. Multidiscip. Optim.*, vol. 47, no. 4, pp. 493–505, 2013.

[55] J. Jensen, O. Sigmund, L. H. Frandsen, P. I. Borel, A. Harpoth, and M. Kristensen, "Topology design and fabrication of an efficient double 90^0 photonic crystal waveguide bend," *IEEE Photon. Technol. Lett.*, vol. 17, no. 6, pp. 1202–1204, 2005.

[56] S. Yamasaki, T. Nomura, A. Kawamoto, K. Sato, and S. Nishiwaki, "A level set-based topology optimization method targeting metallic waveguide design problems," *Int. J. Num. Meth. Eng.*, vol. 87, no. 9, pp. 844–868, 2011.

[57] K. Yee, "Numerical solution of initial boundary value problems involving Maxwell's equations in isotropic media," *IEEE Trans. Antennas Propag.*, vol. 14, no. 3, pp. 302 –307, May 1966.

[58] G. Mur, "Absorbing boundary conditions for the finite-difference approximation of the time-domain electromagnetic-field equations," *IEEE Trans. Electromagn. Compat.*, vol. 23, no. 4, pp. 377–382, 1981.

[59] J.-P. Berenger, "A perfectly matched layer for the absorption of electromagnetic waves," *J. Comput. Phys.*, vol. 114, no. 2, pp. 185–200, 1994.

[60] S. Gedney, "An anisotropic perfectly matched layer-absorbing medium for the truncation of FDTD lattices," *IEEE Trans. Antennas Propag.*, vol. 44, no. 12, pp. 1630 –1639, Dec. 1996.

[61] J. Fang and Z. Wu, "Generalized perfectly matched layer for the absorption of propagating and evanescent waves in lossless and lossy media," *IEEE Trans. Microw. Theory Tech.*, vol. 44, no. 12, pp. 2216–2222, Dec. 1996.

[62] N. Farahat and R. Mittra, "Analysis of frequency selective surfaces using the finite difference time domain (FDTD) method," in *IEEE AP-S Int. Symp.*, vol. 2, 2002, pp. 568–571.

[63] A. Taflove and S. Hagness, *Computational Electrodynamics: The Finite-Difference Time-Domain Method*, 3rd ed. Artech House, 2005.

[64] A. Elsherbeni and V. Demir, *The Finite Difference Time Domain Method for Electromagnetics: With MATLAB Simulations*. SciTech Publishing, Inc., 2009.

[65] U. S. Inan and R. A. Marshall, *Numerical Electromagnetics: The FDTD Method*. Cambridge University Press, 2011.

[66] B. P. Lathi, *Modern Digital and Analog Communication Systems*, 3rd ed. Oxford University Press, 1998.

[67] K. Svanberg, "A class of globally convergent optimization methods based on conservative convex separable approximations," *SIAM J. Optim.*, vol. 12, no. 2, pp. 555–573, 2002.

[68] A. Foudazi, H. Hassani, and S. Nezhad, "Small UWB planar monopole antenna with added GPS/GSM/WLAN bands," *IEEE Trans. Antennas Propag.*, vol. 60, no. 6, pp. 2987–2992, 2012.

[69] A. Ruengwaree, A. Ghose, and G. Kompa, "A novel UWB rugby-ball antenna for near-range microwave radar system," *IEEE Trans. Microw. Theory Tech.*, vol. 54, no. 6, pp. 2774–2779, 2006.

[70] S. Noghanian and L. Shafai, “Control of microstrip antenna radiation characteristics by ground plane size and shape,” *IEE Proc. on Microw. Antennas Propag.*, vol. 145, no. 3, pp. 207–212, 1998.

[71] E. El-Deen, S. Zainud-Deen, H. Sharshar, and M. A. Binyamin, “The effect of the ground plane shape on the characteristics of rectangular dielectric resonator antennas,” in *IEEE AP-S Int. Symp.*, 2006, pp. 3013–3016.

[72] S. Best, “The significance of ground-plane size and antenna location in establishing the performance of ground-plane-dependent antennas,” *IEEE Antennas Propag. Mag.*, vol. 51, no. 6, pp. 29–43, 2009.

[73] K. Mandal and P. Sarkar, “High gain wide-band U-shaped patch antennas with modified ground planes,” *IEEE Trans. Antennas Propag.*, vol. 61, no. 4, pp. 2279–2282, 2013.

[74] P. Gibson, “The Vivaldi aerial,” in *9th European Microwave Conference*, Sep. 1979, pp. 101–105.

[75] J. Langley, P. Hall, and P. Newham, “Novel ultrawide-bandwidth Vivaldi antenna with low crosspolarisation,” *Electron. Lett.*, vol. 29, no. 23, pp. 2004–2005, Nov. 1993.

[76] J.-H. Bang and B.-C. Ahn, “Coaxial-to-circular waveguide transition with broadband mode-free operation,” *Electron. Lett.*, vol. 50, no. 20, pp. 1453–1454, Sep. 2014.

[77] W. Yi, E. Li, G. Guo, and R. Nie, “An X-band coaxial-to-rectangular waveguide transition,” in *ICMTCE 2011*, May 2011, pp. 129–131.

[78] N. Tako, E. Levine, G. Kabilo, and H. Matzner, “Investigation of thick coax-to-waveguide transitions,” in *EuCAP 2014*, Apr. 2014, pp. 908–911.